Analysis of Heat Transfer in Consecutive Variable Cross-Sectional Domains: Applications in Biological Media and Thermal Management

Shadi Mahjoob

Kambiz Vafai[1]
e-mail: vafai@engr.ucr.edu

Department of Mechanical Engineering,
University of California,
Riverside, CA 92521

Temperature prescription and control is important within biological media and in bioheat transport applications such as in hyperthermia cancer treatment in which the unhealthy tissue/organ is subject to an imposed heat flux. Thermal transport investigation and optimization is also important in designing heat management devices and small-scale porous-filled-channels utilized in electronic and biomedical applications. In this work, biological media or the stated heat management devices with a nonuniform geometry are modeled analytically as a combination of convergent, uniform and/or divergent configurations. The biological media is represented as blood saturated porous tissue matrix while incorporating cells and interstices. Two primary models, namely, adiabatic and constant temperature boundary conditions, are employed and the local thermal nonequilibrium and an imposed heat flux are fully accounted for in the presented analytical expressions. Fluid and solid temperature distributions and Nusselt number correlations are derived analytically for variable cross-sectional domain represented by convergent, divergent, and uniform or any combination thereof of these geometries while also incorporating internal heat generation in fluid and/or solid. Our results indicate that the geometrical variations have a substantial impact on the temperature field within the domain and on the surface with an imposed heat flux. It is illustrated that, the temperature distribution within a region of interest can be controlled by a proper design of the multisectional domain as well as proper selection of the porous matrix. These comprehensive analytical solutions are presented for the first time, to the best of the authors' knowledge in literature.
[DOI: 10.1115/1.4002303]

Keywords: bioheat, nonuniform geometry, electronic and biomedical applications, variable area domain, porous media

1 Introduction

Analyses of temperature distribution and heat transfer through small-scale channels subject to an imposed heat flux are key issues in a variety of applications such as biomedical devices [1–5], cooling of electronic devices and heat pipe technology [6–13]. The channels can be filled with porous inserts, which have been shown to be highly effective in heat transfer enhancement and thermal management [14–19] by providing an extensive surface area between solid and fluid phases.

Temperature control and prescription is crucial in bioheat transport applications such as in hyperthermia cancer treatment, where the unhealthy tissue/organ is subject to an imposed heat flux during the course of the treatment. The biological media can be modeled as blood saturated porous tissue matrix consisting of interstices and cells. Mahjoob and Vafai [20,21] investigated transport through biological media for uniform single and multilayer tissue matrix structures. They had investigated several important parameters affecting transport through the biological media such as volume fraction of the vascular space, organ/tissue depth, imposed hyperthermia heat flux, metabolic heat generation, and body core temperature. Aspects related to modeling in porous media incorporated in this work are given in Refs. [22–30]. Nield and Kuznetsov [31] performed an investigation related to forced convection in a channel filled with a porous medium with counterflow.

The geometrical configuration of the channels is also of importance when designing these heat management devices. The temperature distribution on the surface of the devices connected to the channels can be controlled and optimized utilizing proper uniform and nonuniform (convergent or divergent) geometries or a combination thereof. Mahjoob and Vafai [8] developed an analytical solution for a convergent single channel while incorporating the local thermal nonequilibrium condition. The effects of several pertinent parameters on the temperature distribution and heat transfer coefficient such as inclination angle, interfacial fluid-solid heat exchange, ratio of fluid to solid effective thermal conductivities, and imposed heat flux were investigated [8].

In the present work, the effect of a geometrically nonuniform domain is studied by modeling it analytically as a sequential series of convergent, divergent and/or uniform configurations. For the first time, to the best of the authors' knowledge,fluid and solid temperature distributions and the heat transfer coefficient are derived for variable cross-sectional media such as convergent, divergent, and uniform channels filled with a porous medium or any combination thereof of these geometries while incorporating the possibility of existence of internal heat generation in fluid or solid or both phases as well as the local thermal nonequilibrium condition.

[1]Corresponding author.

Manuscript received May 29, 2010; final manuscript received July 31, 2010; published online September 27, 2010. Assoc. Editor: Peter Vadasz.

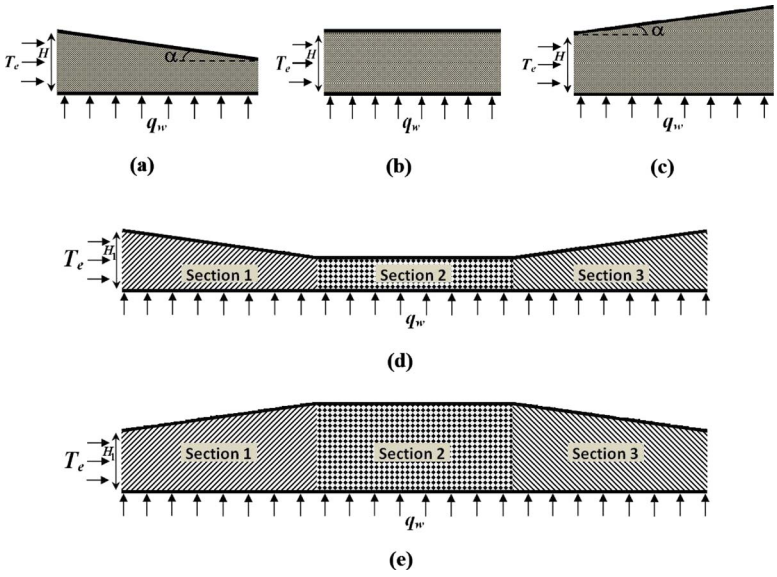

Fig. 1 Schematic diagram of a channel filled with a porous medium subject to a constant heat flux on one side and either an adiabatic or a constant temperature wall on the other side (at the upper wall): (*a*) convergent channel, (*b*) uniform channel, (*c*) divergent channel, (*d*) variable cross-sectional domain made of convergent-uniform-divergent sections, and (*e*) variable cross-sectional domain made of divergent-uniform-convergent sections

2 Modeling and Formulation

2.1 Problem Description. In this work, variable cross-sectional media are represented by channels with nonuniform (convergent or divergent) and uniform geometries filled with a porous medium subject to forced convection and a uniform heat flux. These domains can represent either a biological media or small-scale heat management devices, where the temperature distribution and heat transfer aspects are analyzed within them. Special consideration is given at the intersection of two consecutive sections to ensure proper accounting of the interface boundary conditions. The schematic diagrams of the type of geometries that were analyzed in this work are presented in Figs. 1(*a*)–1(*c*). The analytical solutions that are obtained in this work can be used for any combination of these geometries such as those shown in Figs. 1(*d*) and 1(*e*). In principal, various variable area media such as biological tissue can be modeled with convergent and/or divergent modular sections such as those shown in Figs. 1(*d*) and 1(*e*).

One side of each modular component is subject to a constant heat flux and the other side is subject to either an adiabatic or a constant temperature condition while accounting for internal heat generation from the solid or fluid phases (or both) within the variable cross-sectional domain. It should be noted that the results presented for the adiabatic boundary are also applicable for a symmetric domain in which the heat flux is imposed from both sides of the module. In Fig. 1, H refers to the thickness at the entrance of each section of the module while that of the first section of a multicomponent module is referred to by H_1. The angle between the inclined wall and the longitudinal direction is α. Parameter x_0 is the longitudinal coordinate of the starting point of each section in a multicomponent channel or that of a single-section channel. Flow is considered to be thermally and hydraulically fully developed within an isotropic and homogeneous porous medium. Radiation and natural convection are neglected while assuming constant properties.

2.2 Governing Equations. The governing energy equations for fluid and solid phases, incorporating local thermal nonequilibrium condition and fluid and solid internal heat generations are as follows [20–30].

Fluid phase

$$k_{f,\text{eff}}\nabla_y^2\langle T_f\rangle^f + h_{sf}a_{sf}(\langle T_s\rangle^s - \langle T_f\rangle^f) + \varepsilon\dot{q}_f = \varepsilon\rho c_p\langle u\rangle^f\frac{\partial\langle T_f\rangle^f}{\partial x} \quad (1)$$

Solid phase

$$k_{s,\text{eff}}\nabla_y^2\langle T_s\rangle^s - h_{sf}a_{sf}(\langle T_s\rangle^s - \langle T_f\rangle^f) + (1-\varepsilon)\dot{q}_s = 0 \quad (2)$$

where

$$k_{f,\text{eff}} = \varepsilon k_f + k_{f,\text{dis}} \quad (3)$$

$$k_{s,\text{eff}} = (1-\varepsilon)k_s \quad (4)$$

and parameters $k_{f,\text{eff}}$, $k_{s,\text{eff}}$, k_f, k_s, $k_{f,\text{dis}}$, ε, ρ, and c_p are the fluid and solid effective and regular thermal conductivities, fluid dispersion thermal conductivity, porosity, fluid density, and specific heat capacity, respectively. $\langle T_f\rangle^f$, $\langle T_s\rangle^s$, $\langle u\rangle^f$, $\dot{q}_f$, and $\dot{q}_s$ represent the intrinsic phase average fluid and solid temperatures, intrinsic fluid phase average velocity, and internal heat generation within the fluid and solid phases, respectively. The fluid-solid interfacial heat transfer coefficient is represented by h_{sf} and the specific surface area by a_{sf}.

2.3 Normalization. The governing Eqs. (1) and (2) are normalized by using the following nondimensional variables.

$$\eta = \frac{y}{H \pm (x-x_0)\tan\alpha} \quad \theta = \frac{k_{s,\text{eff}}(\langle T\rangle - T_w)}{q_w H} \quad \kappa = \frac{k_{f,\text{eff}}}{k_{s,\text{eff}}}$$

$$\psi = \frac{(H \pm (x-x_0)\tan\alpha)^2}{H^2} \quad \Phi = \frac{(1-\varepsilon)H\dot{q}}{q_w} \quad \text{Bi} = \frac{h_{sf}a_{sf}H^2}{k_{s,\text{eff}}} \quad (5)$$

Note that the sign $\pm$ in this work refers to whether the modular section is a divergent channel (+) or a convergent one (−). For a multisectional domain, H is the thickness of each section's entrance. In Eq. (5), parameters η and θ represent the nondimensional transverse coordinate and nondimensional temperature, re-

spectively. Parameter κ represents the ratio of fluid to solid effective thermal conductivities and the parameter ψ is the upper wall shape factor. The parameter Φ is the nondimensional internal heat generation. The parameter Bi is an equivalent Biot number indicating the ratio of the conduction resistance within the solid matrix to the thermal resistance corresponding to the internal convective heat exchange between the solid matrix and the fluid phase [29]. For brevity, the intrinsic volume averaging sign ($\langle\ \rangle$) is dropped in the following sections.

2.4 Normalized Governing Equations and Boundary Conditions. Utilizing Eq. (5) and after some modifications, the governing Eqs. (1) and (2) are presented as

$$\kappa\frac{\partial^4\theta_f}{\partial\eta^4}-(1+\kappa)\mathrm{Bi}\psi\left(\frac{\partial^2\theta_f}{\partial\eta^2}\right)=-(1+\Gamma)\mathrm{Bi}\psi^{3/2} \tag{6}$$

$$\kappa\frac{\partial^4\theta_s}{\partial\eta^4}-(1+\kappa)\mathrm{Bi}\psi\left(\frac{\partial^2\theta_s}{\partial\eta^2}\right)=-(1+\Gamma)\mathrm{Bi}\psi^{3/2} \tag{7}$$

where Γ is zero for the adiabatic boundary condition (model I). For the constant temperature boundary condition (model II), Γ is represented by

$$\Gamma=\frac{1}{q_w}\left(k_{f,\mathrm{eff}}\frac{\partial T_f}{\partial y}+k_{s,\mathrm{eff}}\frac{\partial T_s}{\partial y}\right)\Bigg|_{y=H\pm(x-x_0)\tan(\alpha)} \tag{8}$$

The imposed constant heat flux (q_w) is distributed between the fluid and solid phases based on the physical values of their effective thermal conductivities and temperature gradients [8,20,21,28–30]. Boundary conditions are normalized using Eq. (5) and additional boundary conditions are obtained by evaluating the second or third order derivatives of θ_f and θ_s at the boundaries. This results in

$$\theta_f|_{\eta=0}=\theta_s|_{\eta=0}=0 \tag{9}$$

$$\left.\frac{\partial^2\theta_f}{\partial\eta^2}\right|_{\eta=0}=\frac{(1+\Gamma)\psi^{1/2}+\psi\Phi_s}{\kappa} \tag{10}$$

$$\left.\frac{\partial^2\theta_s}{\partial\eta^2}\right|_{\eta=0}=-\psi\Phi_s \tag{11}$$

2.4.1 Model I: Adiabatic Boundary Condition.

$$\left.\frac{\partial\theta_f}{\partial\eta}\right|_{\eta=1}=\left.\frac{\partial\theta_s}{\partial\eta}\right|_{\eta=1}=0 \tag{12}$$

$$\left.\frac{\partial^3\theta_f}{\partial\eta^3}\right|_{\eta=1}=\left.\frac{\partial^3\theta_s}{\partial\eta^3}\right|_{\eta=1}=0 \tag{13}$$

2.4.2 Model II: Constant Temperature Boundary Condition.

$$\theta_f|_{\eta=1}=\theta_s|_{\eta=1}=\theta_c \tag{14}$$

$$\left.\frac{\partial^2\theta_f}{\partial\eta^2}\right|_{\eta=1}=\frac{(1+\Gamma)\psi^{1/2}+\psi\Phi_s}{\kappa} \tag{15}$$

$$\left.\frac{\partial^2\theta_s}{\partial\eta^2}\right|_{\eta=1}=-\psi\Phi_s \tag{16}$$

where

$$\theta_c=\frac{k_{s,\mathrm{eff}}(T_c-T_w)}{q_wH} \tag{17}$$

2.5 Fluid, Solid, and Wall Temperature Distributions. The fluid and solid phase temperature distributions are derived by solving the presented governing equations and utilizing the given Neumann and Dirichlet boundary conditions. After a lengthy analysis, the temperature distributions for the fluid and the solid phases are derived for the adiabatic (model I) and constant temperature (model II) boundary conditions, which are applied at the upper wall of the channel.

2.5.1 Model I: Adiabatic Boundary Condition.

$$\theta_f=\frac{\psi^{1/2}}{1+\kappa}\left(\eta\left(\frac{\eta}{2}-1\right)-\frac{1+(1+\kappa)\psi^{1/2}\Phi_s}{(1+\kappa)\mathrm{Bi}\psi}\left\{1-\frac{e^{\lambda\eta}+e^{\lambda(2-\eta)}}{1+e^{2\lambda}}\right\}\right) \tag{18}$$

$$\theta_s=\frac{\psi^{1/2}}{1+\kappa}\left(\eta\left(\frac{\eta}{2}-1\right)+\frac{\kappa(1+(1+\kappa)\psi^{1/2}\Phi_s)}{(1+\kappa)\mathrm{Bi}\psi}\left\{1-\frac{e^{\lambda\eta}+e^{\lambda(2-\eta)}}{1+e^{2\lambda}}\right\}\right) \tag{19}$$

where

$$\lambda=\sqrt{\mathrm{Bi}\psi(1+\kappa)/\kappa} \tag{20}$$

As such, the temperature difference between the solid and the fluid phases and the wall surface temperature, which is subject to an imposed heat flux, can be written as

$$\Delta\theta=\theta_s-\theta_f=\frac{1+(1+\kappa)\psi^{1/2}\Phi_s}{(1+\kappa)\psi^{1/2}\mathrm{Bi}}\left(1-\frac{e^{\lambda\eta}+e^{\lambda(2-\eta)}}{1+e^{2\lambda}}\right) \tag{21}$$

$$\begin{aligned}T_w=\frac{q_w}{k_{f,\mathrm{eff}}+k_{s,\mathrm{eff}}}\Bigg(&\frac{H\pm(x-x_0)\tan(\alpha)}{3}\\&+\frac{k_{s,\mathrm{eff}}q_w+(1-\varepsilon)\dot{q}_s(k_{f,\mathrm{eff}}+k_{s,\mathrm{eff}})[H\pm(x-x_0)\tan(\alpha)]}{h_{sf}a_{sf}(1+\kappa)[H\pm(x-x_0)\tan(\alpha)]q_w}\\&\times\left\{1-\frac{1}{\lambda}\frac{e^{2\lambda}-1}{e^{2\lambda}+1}\right\}\Bigg)\\&+\frac{q_w+(\varepsilon\dot{q}_f+(1-\varepsilon)\dot{q}_s)[H\pm0.5(x-x_0)\tan(\alpha)]}{\rho c_p u_i H}(x-x_0)+T_i\end{aligned} \tag{22}$$

2.5.2 Model II: Constant Temperature Boundary Condition. The governing equations (6) and (7) are solved while utilizing the boundary conditions for a constant temperature upper wall. This results in the fluid and solid temperature profiles, which can be rewritten using Eq. (8) so that the presented solution will be independent of the term Γ. As such the term Γ and the fluid and solid temperature distributions are derived as

$$\Gamma=\frac{2(1+\kappa)\theta_c}{\psi^{1/2}}+1 \tag{23}$$

$$\begin{aligned}\theta_f=\frac{1}{1+\kappa}\Bigg(&\eta[(\psi^{1/2}+(1+\kappa)\theta_c)\eta-\psi^{1/2}]\\&-\frac{[2\psi^{1/2}+(1+\kappa)(2\theta_c+\psi\Phi_s)]}{(1+\kappa)\mathrm{Bi}\psi}\left\{1-\frac{e^{\lambda\eta}+e^{\lambda(1-\eta)}}{1+e^{\lambda}}\right\}\Bigg)\end{aligned} \tag{24}$$

$$\begin{aligned}\theta_s=\frac{1}{1+\kappa}\Bigg(&\eta[(\psi^{1/2}+(1+\kappa)\theta_c)\eta-\psi^{1/2}]\\&+\frac{\kappa[2\psi^{1/2}+(1+\kappa)(2\theta_c+\psi\Phi_s)]}{(1+\kappa)\mathrm{Bi}\psi}\left\{1-\frac{e^{\lambda\eta}+e^{\lambda(1-\eta)}}{1+e^{\lambda}}\right\}\Bigg)\end{aligned} \tag{25}$$

$$\Delta\theta = \theta_s - \theta_f = \frac{2\psi^{1/2} + (1+\kappa)(2\theta_c + \psi\Phi_s)}{(1+\kappa)\mathrm{Bi}\psi}\left\{1 - \frac{e^{\lambda\eta} + e^{\lambda(1-\eta)}}{1+e^{\lambda}}\right\} \tag{26}$$

where λ is defined in Eq. (20). The wall temperature, which is subject to an imposed heat flux, is derived to be

$$T_w = \Omega + (T_{w,x=x_0} - \Omega)\exp\left(\frac{-(k_{f,\mathrm{eff}} + k_{s,\mathrm{eff}})(x - x_0)}{\rho c_p u_i H^2\left\{\frac{1}{\mathrm{Bi}(1+\kappa)}\left(1 + \frac{2(1-e^{\lambda_0})}{\lambda_0(1+e^{\lambda_0})}\right) + \frac{1}{3}\right\}}\right) \quad \text{for} \quad \alpha = 0 \tag{27}$$

$$T_w = \exp\left(-\int \Omega_1 d(x - x_0)\right)\left\{\int\left[\exp\left(\int \Omega_1 d(x - x_0)\right)\right] \times \Omega_2 d(x - x_0) + \Omega_3\right\} \quad \text{for} \quad \alpha \neq 0 \tag{28}$$

where

$$\Omega = \frac{H}{k_{f,\mathrm{eff}} + k_{s,\mathrm{eff}}}\{q_w + 0.5H[\varepsilon\dot{q}_f + (1-\varepsilon)\dot{q}_s]\} + T_c \tag{29}$$

$$\Omega_1 = \frac{\frac{(k_{f,\mathrm{eff}} + k_{s,\mathrm{eff}})}{\rho c_p u_i H[H \pm (x - x_0)\tan(\alpha)]} - \frac{\pm 2\tan(\alpha)[H \pm (x - x_0)\tan(\alpha)]}{\mathrm{Bi}\psi^2(1+\kappa)H^2}\left(1 + \frac{2(1-e^{\lambda})}{\lambda(1+e^{\lambda})}\right) - \frac{\pm 2\lambda_0\tan(\alpha)}{\kappa H\lambda^4(1+e^{\lambda})^2}(2\lambda e^{\lambda} - e^{2\lambda} + 1)}{\frac{1}{\mathrm{Bi}\psi(1+\kappa)}\left(1 + \frac{2(1-e^{\lambda})}{\lambda(1+e^{\lambda})}\right) + \frac{1}{3}} \tag{30}$$

$$\Omega_2 = \Omega_1 T_c + \frac{1}{\frac{1}{\mathrm{Bi}\psi(1+\kappa)}\left(1 + \frac{2(1-e^{\lambda})}{\lambda(1+e^{\lambda})}\right) + \frac{1}{3}}\left\{\begin{array}{l} \frac{q_w + 0.5[\varepsilon\dot{q}_f + (1-\varepsilon)\dot{q}_s] \times [H \pm (x - x_0)\tan(\alpha)]}{\rho c_p u_i H} - \\ \frac{\pm\tan(\alpha) q_w H^2}{k_{s,\mathrm{eff}}(1+\kappa)^2\mathrm{Bi}[H \pm (x - x_0)\tan(\alpha)]^2}\left(1 + \frac{2(1-e^{\lambda})}{\lambda(1+e^{\lambda})}\right) - \\ \frac{\pm q_w\lambda_0\tan(\alpha)}{(k_{f,\mathrm{eff}} + k_{s,\mathrm{eff}})\mathrm{Bi}\lambda^2(1+e^{\lambda})^2} \times \left(\frac{2H}{(1+\kappa)[H \pm (x - x_0)\tan(\alpha)]} + \Phi_s\right) \times \\ (2\lambda e^{\lambda} - e^{2\lambda} + 1) + \frac{\pm q_w\tan(\alpha)}{12(k_{f,\mathrm{eff}} + k_{s,\mathrm{eff}})} \end{array}\right\} \tag{31}$$

Ω_3 can be evaluated utilizing the following boundary condition:

$$T_w|_{x=x_0} = T_{w,x=x_0} \tag{32}$$

For a single module domain or for the first component of a multicomponent domain, $T_{w,x=x_0}$ can be evaluated from the following equation. This value also indicates the wall temperature at the channel's entrance ($T_{w,e}$).

$$T_{w,x=x_0} = T_{w,e} = \frac{\frac{2k_{s,\mathrm{eff}}}{q_w H}T_c + \frac{2}{1+\kappa} + \Phi_s}{\frac{\mathrm{Bi}(1+\kappa)}{\mathrm{Bi}(1+\kappa)}\left(1 + \frac{2(1-e^{\lambda_0})}{\lambda_0(1+e^{\lambda_0})}\right) + \frac{k_{s,\mathrm{eff}}}{q_w H}\left(T_i - \frac{T_c}{3}\right) + \frac{1}{6(1+\kappa)}}{\frac{2k_{s,\mathrm{eff}}}{3q_w H}\left\{\frac{3}{\mathrm{Bi}(1+\kappa)}\left(1 + \frac{2(1-e^{\lambda_0})}{\lambda_0(1+e^{\lambda_0})}\right) + 1\right\}} \tag{33}$$

and

$$\lambda_0 = \sqrt{\mathrm{Bi}(1+\kappa)/\kappa} \tag{34}$$

For other sections of a multicomponent domain, $T_{w,x=x_0}$ is extracted from the immediate last component of the module under consideration. This process is described in more detail later on.

2.6 Heat Transfer Correlations. The wall heat transfer coefficient is obtained from

$$h_w = \frac{q_w}{T_w - T_{f,m}} \tag{35}$$

The Nusselt number at the channel wall subject to a constant heat flux can be represented as

$$\mathrm{Nu}_w = \frac{h_w D_h}{k_{f,\mathrm{eff}}} = \frac{-2}{\kappa\theta_{f,m}} \tag{36}$$

2.6.1 Model I: Adiabatic Boundary Condition.

$$\mathrm{Nu}_w = \frac{2(1+\kappa)}{\kappa\psi^{1/2}\left(\frac{1}{3} + \frac{1 + (1+\kappa)\psi^{1/2}\Phi_s}{(1+\kappa)\mathrm{Bi}\psi}\left\{1 - \frac{1}{\lambda}\frac{e^{2\lambda} - 1}{e^{2\lambda} + 1}\right\}\right)} \tag{37}$$

2.6.2 Model II: Constant Temperature Boundary Condition.

$$\mathrm{Nu}_w = \frac{2}{\kappa\left(\frac{[2\psi^{1/2} + (1+\kappa)(2\theta_c + \psi\Phi_s)]}{(1+\kappa)^2 \mathrm{Bi}\psi}\left\{1 + \frac{2(1-e^{\lambda})}{\lambda(1+e^{\lambda})}\right\} + \frac{\psi^{1/2}}{6(1+\kappa)} - \frac{\theta_c}{3}\right)} \tag{38}$$

2.7 Simplified Solution Based on Local Thermal Equilibrium Assumption. The energy equation for the one equation model (utilizing the assumption of local thermal equilibrium between fluid and solid phases) can be obtained by adding Eqs. (1) and (2) with the following boundary conditions:

$$\theta|_{\eta=0} = 0 \tag{39}$$

and

$$\left.\frac{\partial\theta}{\partial\eta}\right|_{\eta=1} = 0 \quad \text{for model I: adiabatic boundary condition} \tag{40}$$

$$\theta|_{\eta=1} = \theta_c \quad \text{for model II: constant temperature boundary condition} \tag{41}$$

where θ_c is defined in Eq. (17).

Based on the simplified governing equations and boundary conditions, the following relationships are obtained for the wall temperature, the temperature distribution and the Nusselt number for models I and II.

2.7.1 Model I: Adiabatic Boundary Condition.

$$\theta = \frac{\psi^{1/2}}{1+\kappa}\left(\frac{\eta}{2} - 1\right)\eta \tag{42}$$

$$T_w = \frac{q_w[H \pm (x - x_0)\tan(\alpha)]}{3(k_{f,\mathrm{eff}} + k_{s,\mathrm{eff}})} + \frac{q_w + (\varepsilon\dot{q}_f + (1-\varepsilon)\dot{q}_s)[H \pm 0.5(x - x_0)\tan(\alpha)]}{\rho c_p u_i H}(x - x_0) + T_i \tag{43}$$

$$\mathrm{Nu}_{w,TE} = \frac{6(1+\kappa)}{\kappa\sqrt{\psi}} \tag{44}$$

2.7.2 Model II: Constant Wall Temperature Boundary Condition.

$$\theta = \frac{\eta}{1+\kappa}[(\psi^{1/2} + (1+\kappa)\theta_c)\eta - \psi^{1/2}] \tag{45}$$

$$T_w = \Omega + (T_{w,x=x_0} - \Omega)\exp\left(\frac{-3(k_{f,\mathrm{eff}} + k_{s,\mathrm{eff}})}{\rho c_p u_i H^2}(x - x_0)\right) \quad \text{for} \quad \alpha = 0 \tag{46}$$

$$T_w = T_c + \left(\frac{1}{4(k_{f,\mathrm{eff}} + k_{s,\mathrm{eff}})} \pm \frac{3}{\rho c_p u_i H \tan(\alpha)}\right)\frac{q_w[H \pm (x - x_0)\tan(\alpha)]}{\left(1 \pm \frac{3(k_{f,\mathrm{eff}} + k_{s,\mathrm{eff}})}{\rho c_p u_i H \tan(\alpha)}\right)} + \frac{3[\varepsilon\dot{q}_f + (1-\varepsilon)\dot{q}_s] \times (H \pm (x - x_0)\tan(\alpha))^2}{2\rho c_p u_i H \tan(\alpha)\left(\frac{3(k_{f,\mathrm{eff}} + k_{s,\mathrm{eff}})}{\rho c_p u_i H \tan(\alpha)} \pm 2\right)} + \Omega'\left(\frac{H \pm (x - x_0)\tan(\alpha)}{H}\right)^{\pm(-3(k_{f,\mathrm{eff}} + k_{s,\mathrm{eff}})/(\rho c_p u_i H \tan(\alpha)))} \quad \text{for} \quad \alpha \neq 0 \tag{47}$$

$$\mathrm{Nu}_{w,TE} = \frac{-12(1+\kappa)}{\kappa(2(1+\kappa)\theta_c - \psi^{1/2})} \tag{48}$$

where Ω is defined in Eq. (29) and

$$\Omega' = \frac{3}{2}\left\{\pm\frac{-3q_w H}{2[\rho c_p u_i H \tan(\alpha) \pm 3(k_{f,\mathrm{eff}} + k_{s,\mathrm{eff}})]} \pm \frac{-H^2[\varepsilon\dot{q}_f + (1-\varepsilon)\dot{q}_s]}{2\rho c_p u_i H \tan(\alpha) \pm 3(k_{f,\mathrm{eff}} + k_{s,\mathrm{eff}})} + T_i + T_c\right\} \tag{49}$$

For a single-section module or for the first component of a multicomponent domain, $T_{w,x=x_0}$ can be evaluated from the following equation:

$$T_{w,x=x_0} = T_{w,e} = \frac{1}{2}\left(3T_i - T_c + \frac{q_w H}{2k_{s,\mathrm{eff}}(1+\kappa)}\right) \tag{50}$$

For the subsequent sections of a multicomponent domain, $T_{w,x=x_0}$ is extracted from the immediate last component of the domain under consideration. This process is described in more detail below.

2.8 Special Considerations for Multicomponent Domains. The presented equations for the temperature distributions and the Nusselt number are valid for every section of a multicomponent domain. However, special attention should be given in designating the boundary condition at the entrance of each section after the very first module. The boundary condition, at the interface between two sections should link the data between the two consecutive modules. For instance, the entrance velocity should be adjusted based on the continuity equation. As such, it can be evaluated based on the entrance heights of the consecutive sections as well as the flow velocity at the entrance of the module under consideration. Note that interface height is an important parameter for the value of Biot number for the module under consideration.

Other important parameters are the wall temperature and mean flow temperature at the entrance of a given section. The wall temperature at the entrance ($T_{w,x=x_0}$) can be taken to be the same as the wall temperature at the end of the section immediately preceding it. Then, the mean flow temperature at the entrance of the section can be evaluated from the expressions given below for models I and II.

2.8.1 Model I: Adiabatic Boundary Condition.

$$T_i = \frac{q_w H}{k_{s,\mathrm{eff}}}\theta_{f,m}|_{x=x_0} + T_{w,x=x_0} \tag{51}$$

For local thermal nonequilibrium condition (general form)

$$T_i = \frac{-q_w H}{k_{s,\text{eff}}(1+\kappa)}\left(\frac{1}{3} + \frac{1+(1+\kappa)\Phi_s}{(1+\kappa)\text{Bi}}\left\{1 - \frac{1}{\lambda_0}\frac{e^{2\lambda_0}-1}{e^{2\lambda_0}+1}\right\}\right) + T_{w,x=x_0} \tag{52}$$

and for local thermal equilibrium assumption T_i can be obtained from

$$T_i = \frac{-q_w H}{3k_{s,\text{eff}}(1+\kappa)} + T_{w,x=x_0} \tag{53}$$

2.8.2 Model II: Constant Temperature Boundary Condition. For local thermal nonequilibrium assumption (general form)

$$T_i = \frac{2}{3}\left\{\frac{3}{\text{Bi}(1+\kappa)}\left(1 + \frac{2(1-e^{\lambda_0})}{\lambda_0(1+e^{\lambda_0})}\right) + 1\right\}T_{w,x=x_0} - \frac{q_w H}{6k_{s,\text{eff}}(1+\kappa)} + \frac{T_c}{3} - \frac{2k_{s,\text{eff}}(1+\kappa)T_c + q_w H[2+(1+\kappa)\Phi_s]}{\text{Bi}k_{s,\text{eff}}(1+\kappa)^2}\left(1 + \frac{2(1-e^{\lambda_0})}{\lambda_0(1+e^{\lambda_0})}\right) \tag{54}$$

For local thermal equilibrium assumption T_i can be obtained from

$$T_i = \frac{1}{3}\left(2T_{w,x=x_0} + T_c - \frac{q_w H}{2k_{s,\text{eff}}(1+\kappa)}\right) \tag{55}$$

In Eqs. (51)–(55), T_i should be evaluated based on the values from the downstream component and $T_{w,x=x_0}$ is evaluated based on the wall temperature value at the exit of the upstream component of a multicomponent domain. The channel may compose of several components with different attributes (such as porosity, porous matrix thermal conductivity, specific surface area, and fluid-solid interstitial heat transfer coefficient). However, in the case of a large difference in the physical properties of the components (not the geometry of components), some modifications may be required to achieve an exact matching at the interface due to the discontinuity of the properties.

3 Result and Discussions

The derived analytical solutions are first compared against pertinent available analytical solutions as well as some numerical simulations. Lee and Vafai [29] and Marafie and Vafai [30] investigated forced convection through a channel with an imposed constant heat flux boundary condition. As such, fluid and solid temperature profiles obtained from the present work at zero inclination angle with no internal heat generation are compared with the analytical solutions given by Lee and Vafai [29] and the analytical and numerical results from Marafie and Vafai [30]. These comparisons, which are shown in Fig. 2, display an excellent agreement between the results. The small deviation in numerical results from the analytical ones is due to the usage of a slightly different Darcy number in the numerical investigations [30].

The comprehensive nature of the derived analytical solutions enables one to investigate various multicomponent consecutive, convergent, divergent, or uniform channels. This requires proper accounting of the interface boundaries between the adjacent components of a multicomponent channel. The fluid and solid temperature distributions at different axial locations of some typical multicomponent domains are presented in Figs. 3–5. The inclined angles, entrance thickness of the channel, imposed heat flux, porous matrix properties, flow rate, and fluid properties are similar in these figures. The lower wall of the multicomponent channel is subject to a constant heat flux and the upper wall is subjected to either an adiabatic boundary condition (Figs. 3 and 4) or a constant temperature boundary (Fig. 5). The temperature quantities in these figures, are normalized by the mean flow temperature at the entrance of the channel (T_e) and the entrance thickness of the channel (H_1).

In Fig. 3, a consecutive multicomponent domain is investigated consisting of a convergent (with 5 deg inclination angle), uniform and divergent (with 5 deg inclination angle) sections, respectively. As can be seen in Fig. 3, there is an excellent agreement at the interfaces of the components ($X=5$, $X=10$), between the results obtained from the analytical solution for the upstream and downstream solutions. Comparing Figs. 3(*a*) and 3(*b*) indicate that an increase in specific surface area (a_{sf}) or fluid-solid interstitial heat transfer coefficient (h_{sf}) decreases the temperature difference between solid and fluid phases.

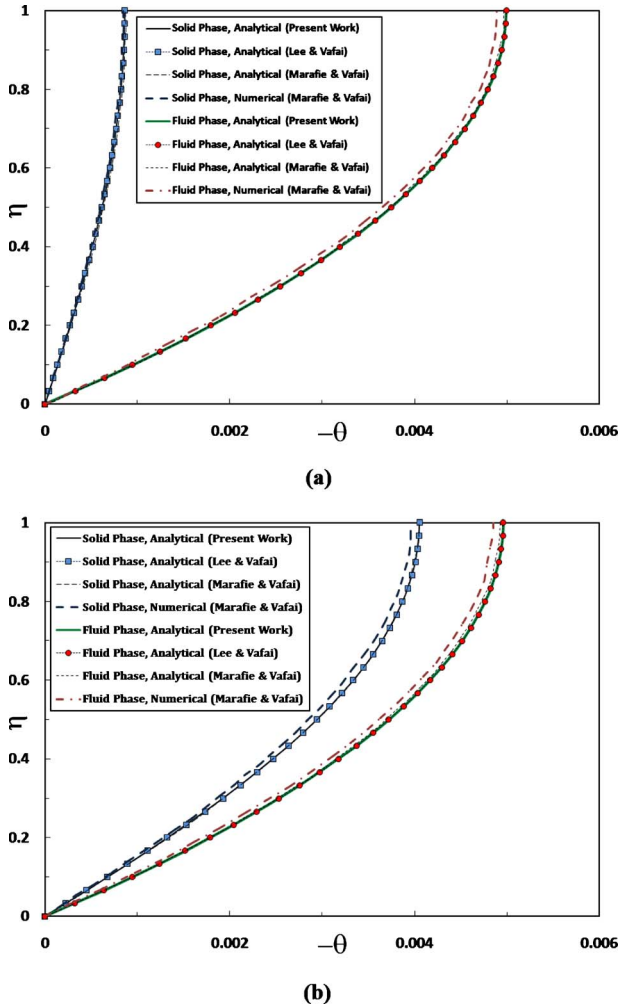

Fig. 2 Comparison of the present analytical fluid and solid temperature distributions at zero inclination angle with the analytical results of Lee and Vafai [29] and analytical-numerical results of Marafie and Vafai [30] for $\kappa=100$, $\dot{q}_f=\dot{q}_s=0$: (*a*) Bi =0.5 and (*b*) Bi=10

Figure 4 displays the fluid and solid temperature distributions at different locations for a divergent-uniform-convergent multisectional channel. The results once again confirm the excellent matching of fluid and solid temperature distributions at the interface between consecutive components ($X=5$, $X=10$). Comparing Figs. 3 and 4, one can see the substantial effect of the variable cross-sectional configurations on the fluid and solid temperature distributions and the wall temperature distribution. These results point out the possibility of controlling the wall temperature and temperature distribution inside each module by a proper design of multicomponent domain type of porous insert and the inlet flow attributes.

Figure 5 displays the temperature distributions at different axial locations of a consecutive multicomponent domain consisting of a convergent (with 5 deg inclination angle), uniform and divergent (with 5 deg inclination angle) modules (Fig. 5(*a*)) and also one

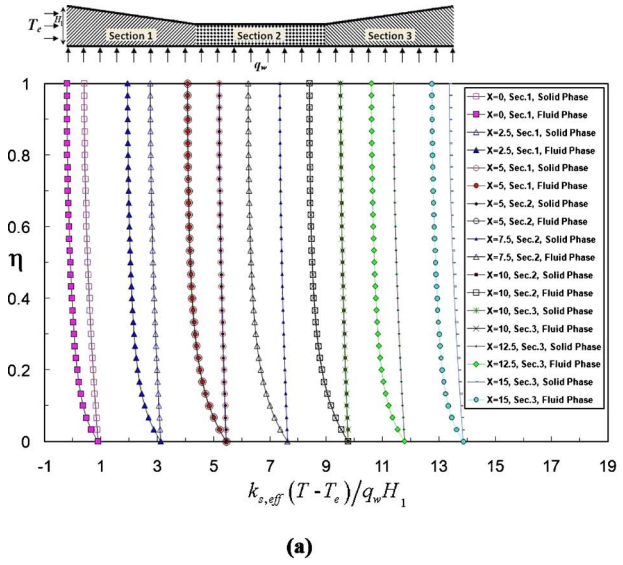

(a)

(b)

Fig. 3 Fluid and solid temperature distributions at different axial locations of a variable cross-sectional domain made of convergent (α=5 deg)-uniform-divergent (α=5 deg) sections, subject to an adiabatic boundary at the upper wall for κ=0.01, $\dot{q}_f=\dot{q}_s$=0: (*a*) Bi=0.5 and (*b*) Bi=10

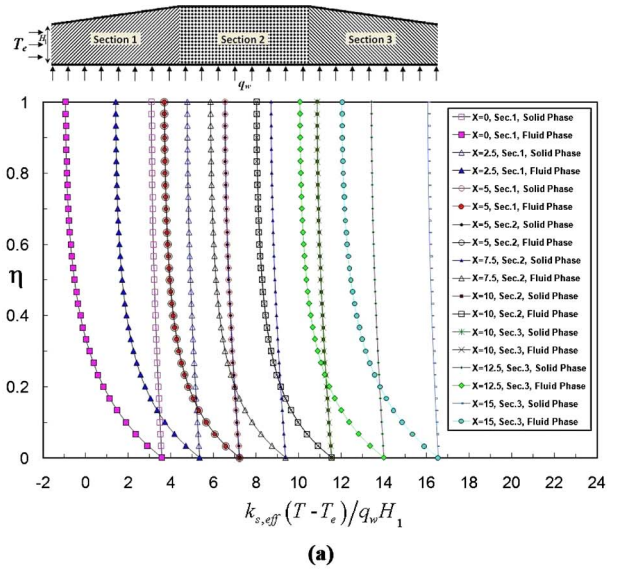

(a)

(b)

Fig. 4 Fluid and solid temperature distributions at different axial locations of a variable cross-sectional domain made of divergent (α=5 deg)-uniform-convergent (α=5 deg) sections, subject to an adiabatic boundary at the upper wall for κ=0.01, $\dot{q}_f=\dot{q}_s$=0: (*a*) Bi=0.5 and (*b*) Bi=10

composed of divergent (with 5 deg inclination angle), uniform and convergent (with 5 deg inclination angle) sections (Fig. 5(*b*)). The lower wall of the multicomponent channel is subject to a constant heat flux and the upper wall has a constant temperature condition and the results are based on utilizing local thermal equilibrium assumption. Once again the results shown in this figure display an excellent matching at the interfaces between different neighboring sections (X=5 and X=10) of the variable cross-sectional domain. The presented analytical results in this work can be valid for a wide range of module thicknesses. It should be noted that the upper wall temperature has an important role on the temperature distribution within each module. For Fig. 5, the upper wall temperature is considered to be the same as that of the mean temperature at the channel's entrance so as to concentrate on the effects of geometry itself rather than the influence of upper wall temperature on the domain under consideration. Since the convergent or divergent inclination angle has a substantial effect on the temperature distribution, a multicomponent channel can be designed to provide the required temperature profile or a uniform temperature on a surface subject to high heat flux such as in electronic cooling applications. The convergent section can cool the domain and the surface efficiently while the temperature can be managed by adding uniform or divergent sections afterwards (Fig. 5(*a*)). As can be seen in Fig. 5(*b*), utilizing a channel with a divergent starting section can considerably reduce the cooling effects of the working flow and the upper wall temperature while a uniform channel can maintain the desired temperature on the surface.

4 Conclusions

A comprehensive analytical investigation of forced convection through a variable cross-sectional domain is carried out. Results obtained form this analysis are pertinent in bioheat transport through variable cross-sectional organ/tissue or in designing thermal management devices as well as in understanding porous medium based heat exchangers. Heat generation within fluid and solid phases is incorporated in the analysis to represent a more adoptive solution. The multisectional domain may compose of

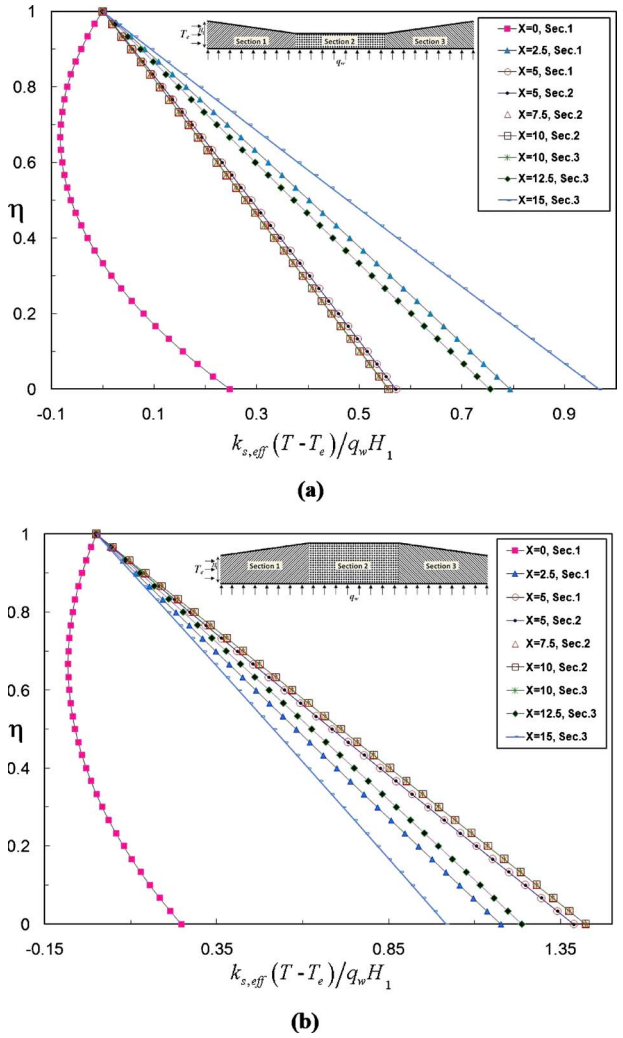

Fig. 5 Temperature distributions at different axial locations of a variable cross-sectional domain made of (*a*) convergent (α =5 deg)-uniform-divergent (α=5 deg) sections; (*b*) divergent (α=5 deg)-uniform-convergent (α=5 deg) sections, subject to a constant temperature at the upper wall, for κ=0.01 and $\dot{q}_f = \dot{q}_s$=0.

variable configurations (convergent, uniform or divergent) with different physical properties such as porosity, specific surface area, fluid-solid interstitial heat transfer coefficient, and different porous matrices. To cover more adoptive and practical conditions, each domain is subject to an imposed heat flux on one side and either a thermally insulated or a constant temperature boundary condition on the other side. The results obtained from the present derived analytical solutions were compared with the available analytical and numerical results in literature and were found to be in a very good agreement. These analytical solutions are presented for the first time, to the best of the authors' knowledge in literature. The temperature profiles were found to match very well at the interface between consecutive sections of a multicomponent domain. The results show that the geometrical variations have a substantial impact on the temperature field within the domain and on the surface with an imposed heat flux. As such, the temperature distributions within the variable cross-sectional domain or at the surface with an imposed heat flux can be controlled by a proper design of the system as well as proper selection of the porous matrix.

Nomenclature

a_{sf} = specific surface area (m^{-1})
Bi = modified Biot number, $h_{sf}a_{sf}H^2/k_{s,\text{eff}}$
c_p = fluid specific heat capacity (J kg^{-1} K^{-1})
D_h = hydraulic diameter of the channel, $2H$ (m)
H = entrance thickness of channel or each section of a multisection channel (m)
H_1 = entrance thickness of the first section of a multisection channel (m)
h_{sf} = fluid-solid interstitial heat transfer coefficient (W m^{-2} K^{-1})
h_w = wall heat transfer coefficient, $q_w/(T_w-T_{f,m})$ (W m^{-2} K^{-1})
k_f = fluid thermal conductivity (W m^{-1} K^{-1})
$k_{f,\text{dis}}$ = fluid dispersion thermal conductivity (W m^{-1} K^{-1})
$k_{f,\text{eff}}$ = effective thermal conductivity of the fluid phase (W m^{-1} K^{-1})
k_s = solid thermal conductivity (W m^{-1} K^{-1})
$k_{s,\text{eff}}$ = effective thermal conductivity of the solid phase (W m^{-1} K^{-1})
Nu_w = Nusselt number at the wall
$\text{Nu}_{w,TE}$ = Nusselt number at the wall for local thermal equilibrium model
q_w = imposed heat flux at the wall (W m^{-2})
$\dot{q}$ = internal heat generation (W m^{-3})
T = temperature (K)
T_e = mean flow temperature at the channel's entrance (K)
$T_{f,m}$ = mean flow temperature (K)
T_c = upper wall constant temperature (K)
T_i = mean flow temperature at the entrance of a single-section channel or at each section of a multicomponent channel (K)
T_w = temperature of the wall subject to an imposed heat flux (K)
$T_{w,e}$ = wall temperature at the entrance of a channel (K)
$T_{w,x=x_0}$ = wall temperature at the entrance of a single-section channel or at each section of a multicomponent channel (K)
u = fluid velocity (m s^{-1})
u_i = fluid velocity at the entrance of a channel or each section of a multicomponent channel (m s^{-1})
x = longitudinal coordinate (m)
x_0 = longitudinal coordinate at the entrance of a channel or each section of a multicomponent channel (m)
X = nondimensional longitudinal coordinate, x/H_1
y = transverse coordinate (m)

Greek Symbols

α = inclination angle
ε = porosity
η = nondimensional transverse coordinate, $y/(H\pm(x-x_0)\tan\alpha)$
κ = ratio of the effective fluid thermal conductivity to that of the solid, $k_{f,\text{eff}}/k_{s,\text{eff}}$
λ = parameter, $\sqrt{\text{Bi}\psi/(1+\kappa)/\kappa}$
λ_0 = parameter, $\sqrt{\text{Bi}(1+\kappa)/\kappa}$
ρ = fluid density (kg m^{-3})
Γ = parameter used in model II: constant temperature boundary condition
$\Delta\theta$ = nondimensional temperature difference between solid and fluid phases

θ = nondimensional temperature, $k_{s,\text{eff}}(\langle T\rangle - T_w)/(q_w H)$
θ_c = nondimensional upper wall constant temperature, $k_{s,\text{eff}}(T_c - T_w)/(q_w H)$
$\theta_{f,m}$ = nondimensional fluid mean temperature
Φ = nondimensional internal heat generation, $(1-\varepsilon)H\dot{q}/q_w$
ψ = upper wall shape factor, $(H \pm (x-x_0)\tan\alpha)^2/H^2$
Ω = a dimensional parameter (K)
Ω_1 = a dimensional parameter (m^{-1})
Ω_2 = a dimensional parameter ($m^{-1}K$)
Ω_3 = a dimensional parameter (K)
Ω' = a dimensional parameter (K)

Subscripts/Superscripts

f = fluid phase
f,m = fluid mean
c = constant temperature wall
eff = effective property
s = solid phase
w = wall subject to an imposed heat flux

Symbols

$+$ = applied in equations for a divergent channel wherever $\pm$ sign is utilized
$-$ = applied in equations for a convergent channel wherever $\pm$ sign is utilized
$\langle\ \rangle$ = intrinsic volume average of a quantity

References

[1] Yoon, D. S., Lee, Y. S., Lee, Y., Cho, H. J., Sung, S. W., Oh, K. W., Cha, J., and Lim, G., 2002, "Precise Temperature Control and Rapid Thermal Cycling in a Micromachined DNA Polymerase Chain Reaction Chip," J. Micromech. Microeng., **12**, pp. 813–823.
[2] Lee, D. S., Tsai, C. Y., Yuan, W. H., Chen, P. J., and Chen, P. H., 2004, "A New Thermal Cycling Mechanism for Effective Polymerase Chain Reaction in Microliter Volumes," Microsyst. Technol., **10**, pp. 579–584.
[3] Mahjoob, S., Vafai, K., and Beer, N. R., 2008, "Rapid Microfluidic Thermal Cycler for Polymerase Chain Reaction Nucleic Acid Amplification," Int. J. Heat Mass Transfer, **51**(9–10), pp. 2109–2122.
[4] Hühmer, A. F. R., and Landers, J. P., 2000, "Noncontact Infrared-Mediated Thermocycling for Effective Polymerase Chain Reaction Amplification of DNA in Nanoliter Volumes," Anal. Chem., **72**(21), pp. 5507–5512.
[5] Swerdlow, H., Jones, B. J., and Wittwer, C. T., 1997, "Fully Automated DNA Reaction and Analysis in a Fluidic Capillary Instrument," Anal. Chem., **69**(5), pp. 848–855.
[6] Zhao, C. Y., and Lu, T. J., 2002, "Analysis of Microchannel Heat Sinks for Electronics Cooling," Int. J. Heat Mass Transfer, **45**(24), pp. 4857–4869.
[7] Fedorov, A. G., and Viskanta, R., 2000, "Three-Dimensional Conjugate Heat Transfer in the Microchannel Heat Sink for Electronic Packaging," Int. J. Heat Mass Transfer, **43**(3), pp. 399–415.
[8] Mahjoob, S., and Vafai, K., 2009, "Analytical Characterization and Production of an Isothermal Surface for Biological and Electronics Applications," ASME J. Heat Transfer, **131**(5), p. 052604.
[9] Kim, S. J., 2004, "Methods for Thermal Optimization of Microchannel Heat Sinks," Heat Transfer Eng., **25**(1), pp. 37–49.
[10] Vasiliev, L. L., 2008, "Micro and Miniature Heat Pipes—Electronic Component Coolers," Appl. Therm. Eng., **28**(4), pp. 266–273.
[11] Udell, K. S., 1985, "Heat Transfer in Porous Media Considering Phase Change and Capillarity—The Heat Pipe Effect," Int. J. Heat Mass Transfer, **28**(2), pp. 485–495.
[12] Vafai, K., and Wang, W., 1992, "Analysis of Flow and Heat Transfer Characteristics of an Asymmetrical Flat Plate Heat Pipe," Int. J. Heat Mass Transfer, **35**, pp. 2087–2099.
[13] Vafai, K., Zhu, N., and Wang, W., 1995, "Analysis of Asymmetric Disk-Shaped and Flat Plate Heat Pipes," ASME J. Heat Transfer, **117**, pp. 209–218.
[14] Mahjoob, S., and Vafai, K., 2008, "A Synthesis of Fluid and Thermal Transport Models for Metal Foam Heat Exchangers," Int. J. Heat Mass Transfer, **51**(15–16), pp. 3701–3711.
[15] Hunt, M. L., and Tien, C. L., 1988, "Effects of Thermal Dispersion on Forced Convection in Fibrous Media," Int. J. Heat Mass Transfer, **31**(2), pp. 301–309.
[16] Zhao, C. Y., Kim, T., Lu, T. J., and Hodson, H. P., 2004, "Thermal Transport in High Porosity Cellular Metal Foams," J. Thermophys. Heat Transfer, **18**(3), pp. 309–317.
[17] Boomsma, K., Poulikakos, D., and Zwick, F., 2003, "Metal Foams as Compact High Performance Heat Exchangers," J. Mech. Mater., **35**, pp. 1161–1176.
[18] Ebara, S., Toda, S., and Hashizume, H., 2000, "Application of Porous Matrix to High Heat Load Removal System," Heat Mass Transfer, **36**, pp. 273–276.
[19] Rachedi, R., and Chikh, S., 2001, "Enhancement of Electronic Cooling by Insertion of Foam Materials," Heat Mass Transfer, **37**, pp. 371–378.
[20] Mahjoob, S., and Vafai, K., 2009, "Analytical Characterization of Heat Transfer Through Biological Media Incorporating Hyperthermia Treatment," Int. J. Heat Mass Transfer, **52**(5–6), pp. 1608–1618.
[21] Mahjoob, S., and Vafai, K., 2010, "Analysis of Bioheat Transport Through a Dual Layer Biological Media," ASME J. Heat Transfer, **132**, p. 031101.
[22] Vafai, K., and Tien, C. L., 1981, "Boundary and Inertia Effects on Flow and Heat Transfer in Porous Media," Int. J. Heat Mass Transfer, **24**, pp. 195–203.
[23] Quintard, M., and Whitaker, S., 2000, "Theoretical Analysis of Transport in Porous Media," *Handbook of Porous Media*, K. Vafai, ed., Marcel Dekker, New York, pp. 1–52.
[24] Khaled, A.-R. A., and Vafai, K., 2003, "The Role of Porous Media in Modeling Flow and Heat Transfer in Biological Tissues," Int. J. Heat Mass Transfer, **46**, pp. 4989–5003.
[25] Vafai, K., and Tien, H. C., 1989, "A Numerical Investigation of Phase Change Effects in Porous Materials," Int. J. Heat Mass Transfer, **32**, pp. 1261–1277.
[26] Amiri, A., and Vafai, K., 1994, "Analysis of Dispersion Effects and Non-Thermal Equilibrium, Non-Darcian, Variable Porosity Incompressible Flow through Porous Medium," Int. J. Heat Mass Transfer, **37**, pp. 939–954.
[27] Nield, D. A., and Bejan, A., 2006, *Convection in Porous Media*, Springer, New York.
[28] Alazmi, B., and Vafai, K., 2002, "Constant Wall Heat Flux Boundary Conditions in Porous Media Under Local Thermal Non-Equilibrium Conditions," Int. J. Heat Mass Transfer, **45**, pp. 3071–3087.
[29] Lee, D. Y., and Vafai, K., 1999, "Analytical Characterization and Conceptual Assessment of Solid and Fluid Temperature Differentials in Porous Media," Int. J. Heat Mass Transfer, **42**, pp. 423–435.
[30] Marafie, A., and Vafai, K., 2001, "Analysis of Non-Darcian Effects on Temperature Differentials in Porous Media," Int. J. Heat Mass Transfer, **44**, pp. 4401–4411.
[31] Nield, D. A., and Kuznetsov, A. V., 2008, "A Bioheat Transfer Model: Forced Convection in a Channel Occupied by a Porous Medium With Counterflow," Int. J. Heat Mass Transfer, **51**, pp. 5534–5541.